Journal of Cerebral Blood Flow & Metabolism (2011) 31, 2041–2053

www.jcbfm.com

T_1- and T_2^*-dominant extravasation correction in DSC-MRI: Part I—theoretical considerations and implications for assessment of tumor hemodynamic properties

Atle Bjornerud[1,2], A Gregory Sorensen[3], Kim Mouridsen[3,4] and Kyrre E Emblem[1,3]

[1]*The Intervention Centre, Rikshospitalet, Oslo University Hospital, Oslo, Norway;* [2]*Department of Physics, University of Oslo, Oslo, Norway;* [3]*A A Martinos Center for Biomedical Imaging, Massachusetts General Hospital and Harvard Medical School, Boston, Massachusetts, USA;* [4]*Center of Functionally Integrative Neuroscience, University of Aarhus, Aarhus, Denmark*

We present a novel contrast agent (CA) extravasation-correction method based on analysis of the tissue residue function for assessment of multiple hemodynamic parameters. The method enables semiquantitative determination of the transfer constant and can be used to distinguish between T_1- and T_2^*-dominant extravasation effects, while being insensitive to variations in tissue mean transit time (MTT). Results in 101 patients with confirmed glioma suggest that leakage-corrected absolute cerebral blood volume (CBV) values obtained with the proposed method provide improved overall survival prediction compared with normalized CBV values combined with an established leakage-correction method. Using a standard gradient-echo echo-planar imaging sequence, ~60% and 10% of tumors with detectable CA extravasation mainly exhibited T_1- and T_2^*-dominant leakage effects, respectively. The remaining 30% of leaky tumors had mixed T_1- and T_2^*-dominant effects. Using an MTT-sensitive correction method, our results show that CBV is underestimated when tumor MTT is significantly longer than MTT in the reference tissue. Furthermore, results from our simulations suggest that the relative contribution of T_1- versus T_2^*-dominant extravasation effects is strongly dependent on the effective transverse relaxivity in the extravascular space and may thus be a potential marker for cellular integrity and tissue structure.
Journal of Cerebral Blood Flow & Metabolism (2011) **31,** 2041–2053; doi:10.1038/jcbfm.2011.52; published online 20 April 2011

Keywords: cerebral hemodynamics; kinetic modeling; MRI; neurooncology; perfusion-weighted MRI

Introduction

Quantitative dynamic susceptibility contrast (DSC) magnetic resonance imaging (MRI) introduces many technical challenges related to the reliable detection of the arterial input function (AIF), choice of deconvolution method, and complex *in vivo* dose response (Calamante *et al*, 2002). Furthermore, contrast agent (CA) extravasation is a general problem for all DSC-based MRI methods used for brain tumor assessment because the kinetic models used explicitly assume that the CA remains in the intravascular space (IVS) for the duration of the dynamic acquisition (Lev and Rosen, 1999). Studies have suggested that CA leakage can lead to either overestimation or underestimation of relative cerebral blood volume (rCBV) in tumors with blood–brain-barrier breakdown unless specifically corrected for (Paulson and Schmainda, 2008). Different approaches to limit the error introduced by CA extravasation have been proposed, including use of predosing (Donahue *et al*, 2000), double-echo acquisitions (Uematsu *et al*, 2001; Vonken *et al*, 2000), and parametric modeling (γ-variate fit) of the dynamic response (Rosen *et al*, 1990). Weisskoff *et al* (1994) proposed a correction method in which CA extravasation is estimated in each voxel by determining the voxel-wise deviation from a 'nonleaky' reference tissue response curve. This approach is appealing in that it does not require the use of nonstandard imaging sequences or CA injection schemes, and the method has been shown to improve the diagnostic accuracy of DSC-MRI in glioma grading (Boxerman *et al*, 2006). The potential limitation of the method is that the model assumes that mean transit time (MTT) and bolus arrival time are the same in tumor and nonpathologic tissue. Quarles *et al* (2005) showed that, based on simulations and data in a rat

Correspondence: Professor A Bjørnerud, The Intervention Centre, Oslo University Hospital, N-0027 Oslo, Norway.
E-mail: atle.bjornerud@fys.uio.no
Received 8 December 2010; revised 16 March 2011; accepted 19 March 2011; published online 20 April 2011

gliosarcoma model, the leakage-correction method of Weisskoff *et al* may result in incorrect rCBV values in tumors with significant alteration in the hemodynamic state. On the basis of this observation, they proposed an alternative method in which CA extravasation is accounted for by incorporating a leakage term in the tissue residue function, thereby providing an MTT-insensitive estimate of the transfer constant describing the CA flux between the IVS and extravascular extracellular space (EES). We recently proposed an alternative approach in which the transfer constant is directly determined from the tissue residue function (Bjornerud and Emblem, 2009). This method can be combined with a fully automated approach for quantitative DSC-MRI incorporating automatic slice-wise detection of the AIF and partial volume correction (Bjornerud and Emblem, 2010). From this, a direct estimation of perfusion metrics and MTT-insensitive CA extravasation from the resulting tissue residue function may be derived. The primary aim of our study was to fully expand the development of the proposed MTT-insensitive leakage-correction method from its theoretical basis through data simulations and finally by analysis of clinical DSC data in patients with confirmed glioma.

Theory

Estimation of Tumor Hemodynamic Parameters in the Presence of Contrast Agent Extravasation

Weisskoff *et al* (1994) proposed a correction method, later elaborated by Boxerman *et al* (2006), whereby CA extravasation is estimated in each voxel by determining the voxel-wise deviation from a 'non-leaky' reference tissue response curve:

$$\Delta R2^*(t) \approx K_1 \cdot \overline{\Delta R2^*(t)} - K_2 \int_0^t \overline{\Delta R2^*(t')} dt', \qquad (1)$$

where $\Delta R2^*(t)$ is the measured CA-induced change in transverse relaxation rate ($1/T_2^*$) in the presence of CA extravasation, $\overline{\Delta R2^*(t)}$ the average $\Delta R2^*(t)$ in voxels with no CA extravasation, and K_1 and K_2 the scaling constants for relative blood volume and permeability, respectively. The negative sign of K_2 is attributed to the assumed T_1-dominant CA relaxation effect in the EES. Relative CBV is given by the area under the first-pass response, and it thus follows that leakage-corrected rCBV is given by:

$$\mathrm{rCBV_{corr}} = \mathrm{rCBV} + K_2 \int_0^T dt'' \int_0^{t''} \overline{\Delta R2^*}(t') dt' \qquad (2)$$

This approach will be used as the reference-correction method in this study. One potential limitation of this method is that it explicitly assumes that MTT in a leaky voxel is identical to MTT of the mean tissue response curve (Quarles *et al*, 2005). This can be seen from equation (1) because, in the absence of extravasation, any given response curve should be related to the reference curve by a single scaling constant (K_1). Any deviations in MTT (or CA delay) would thus introduce an incorrect nonzero value of K_2.

An alternative approach accounting for variations in tissue MTT is to estimate CA extravasation from the tissue residue function obtained after AIF deconvolution. In the absence of CA extravasation, tissue flow can be estimated from the convolution integral (Ostergaard *et al*, 1996):

$$C_{\mathrm{t\_iv}}(t) = f \int_0^t R(t) C_{\mathrm{p}}(t-\tau) d\tau, \qquad (3)$$

where C_{p} is the tracer concentration in the plasma and $C_{\mathrm{t\_iv}}$ the tracer concentration in the tissue (confined to the IVS), $R(t)$ the tissue-specific residue function, and f the tissue flow (in units of 1 per sec). Given that CA concentration in blood and tissue can be determined, f and $R(t)$ can be estimated by deconvolution, and perfusion (in units of mL blood/100 g per min) is then given by:

$$\mathrm{CBF} = \frac{H_{\mathrm{c}}}{\rho} f, \qquad (4)$$

where ρ is the tissue density and $H_{\mathrm{c}} = 1 - \mathrm{Hct_{art}} / 1 - \mathrm{Hct_{cap}}$ takes into account differences in hematocrit values in large vessels and capillaries (Rempp *et al*, 1994). The MTT is given by the area under the residue function and, in the absence of CA extravasation, CBV can then be estimated from the central volume principle (Lassen and Perl, 1979):

$$\mathrm{CBV} = \mathrm{CBF} \cdot \mathrm{MTT} = \frac{H_{\mathrm{c}}}{\rho} f \int_0^\infty R(t) dt \qquad (5)$$

If the tracer is not confined to the IVS, CA extravasation can be expressed in terms of a two-compartment model (Larsson *et al*, 1990; Tofts, 1997; Tofts *et al*, 1999):

$$C_{\mathrm{t\_ev}}(t) = K^{\mathrm{trans}} \int_0^t \exp(-K^{\mathrm{trans}}(t-\tau)/v_{\mathrm{e}}) \cdot C_{\mathrm{p}}(\tau) d\tau, \qquad (6)$$

where K^{trans} is the transfer constant describing CA flux from the IVS to the EES, v_{e} the leakage space per unit volume, and $C_{\mathrm{t\_ev}}$ the tracer concentration in the EES.

To estimate both perfusion and permeability from a single acquisition, a combined model of the two processes is required. We base our combined analysis approach on the adiabatic approximation to the tissue homogeneity model (St Lawrence and Lee, 1998). Here, the intravascular response is modeled as a function of both time and distance along the capillaries, and it is assumed that the dynamic time course is separable into an early (fast) vascular phase, followed by a (slow) extravasation phase. The tissue response, including both intravascular

and extravascular responses can then be expressed as:

$$C_{t\_m}(t) = f\int_0^t R(t)C_p(t-\tau)d\tau + K^{trans} \times \int_{T_c}^{t'} \exp(-K^{trans}(\tau - T_c)/v_e) \cdot C_p(t'-\tau)d\tau, \quad (7)$$

where T_c is the capillary transit time of CA, so that $t < T_c$ and $t' \geq T_c$. The combined residue function $H(t)$ scaled by flow and the extravasation transfer constant can then be expressed as:

$$\begin{aligned} H(t) &\approx f \cdot R(t) && 0 \leq t < T_c \\ H(t) &\approx K^{trans} \cdot \exp(-K^{trans}(t-T_c)/v_e) && t \geq T_c \end{aligned} \quad (8)$$

Complete separation of the intravascular and extravasation phase using this model requires $R(t)$ to be a box function, so that $R(t) = 1$ for $0 \leqslant t < T_c$ and $R(t) = 0$ for $t \geqslant T_c$. However, because the intravascular residue function is in reality a monotonically decreasing probability function, the two phases will overlap and T_c is an average transit time (MTT) for all capillary paths. However, for $t >> T_c$, $H(t)$ is dominated by the leakage term and by further assuming limited reflux within the measurement time, T_N, so that $K^{trans}T_N/v_e \ll 1$, we get:

$$H(t) \approx K^{trans} \quad t >> T_c \quad (9)$$

Dose-Response Considerations

In DSC-MRI, CA concentration can only be estimated in relative terms through measurements of change in transverse relaxation rate ($\Delta R2^*$ or $\Delta R2$), which in turn is estimated from measured change in MR signal intensity (SI). In single-shot gradient echo–echo planar imaging (GRE-EPI) sequences used in DSC-MRI, the SI can be approximated by the steady-state expression:

$$\begin{aligned} SI(C) &= M_0 \frac{\sin(\alpha)(1-\exp(-TR \cdot R1(C)))}{1-\cos(\alpha)\exp(-TR \cdot R1(C))} \exp(-TE \cdot R2^*(C)) \\ &= M_0 E1(C) \cdot \exp(-TE \cdot R2^*(C)), \end{aligned} \quad (10)$$

where M_0 is proportional to the equilibrium magnetization, C the CA concentration, $R1$, $R2^*$ the T_1 and T_2^* relaxation rates, respectively, TE the echo time, and α the flip angle. The change in SI caused by CA-induced increase in relaxation rates can then be expressed as:

$$\begin{aligned} \frac{1}{TE}\left[\ln\left(\frac{SI(0)}{SI(C)}\right)\right] &= \Delta R2^*(C) - \frac{1}{TE}\ln\left(\frac{E1(C)}{E1(0)}\right) \\ &= \Delta R2^*_{app}(C), \end{aligned} \quad (11)$$

where $\Delta R2^*$ is the change in T_2^* relaxation rate, $\Delta R2^*_{app}$ the measured apparent change in $\Delta R2^*$ including T_1 effects, and $E1(C) > E1(0)$. In DSC imaging, the T_1 term in equation (11) is commonly assumed to be negligible compared with the much stronger T_2^* relaxation effects for an intravascular CA distribution (Boxerman *et al*, 1995; Kjolby *et al*, 2006). In the case of CA extravasation, T_1 relaxation effects may become significant because of a reduction in CA compartmentalization (reduced T_2^* relaxation) combined with increased distribution volume and water access to the paramagnetic center of the CA (Donahue *et al*, 1997). Hence, the extravascular CA-induced signal change is more difficult to predict, and both T_1 and T_2^* effects may dominate when the CA is present in the EES.

From this, it cannot be assumed that the transfer constant measured from a single-echo DSC-MRI acquisition reflects the underlying K^{trans}. Therefore, we distinguish between the apparent transfer constant, K_a, estimated through measurements of $\Delta R2^*$ combined with the proposed models, and the true transfer constant K^{trans} as defined in equation (6). Using this notation, equation (7) can be written in matrix notation in terms of the measured changes in T_2^* relaxation rates as:

$$Y = A \cdot h \quad (12)$$

where

$$Y = \begin{bmatrix} \Delta R2^*_t(t_0) \\ \Delta R2^*_t(t_1) \\ \vdots \\ \Delta R2^*_t(t_{N-1}) \end{bmatrix} \quad (13)$$

$$A = \Delta t \cdot \begin{bmatrix} \Delta R2^*_a(t_0) & 0 & 0 & 0 \\ \Delta R2^*_a(t_1) & \Delta R2^*_a(t_0) & \cdots & 0 \\ \vdots & \vdots & \ddots & \vdots \\ \Delta R2^*_a(t_{N-1}) & \Delta R2^*_a(t_{N-2}) & \cdots & \Delta R2^*_a(t_0) \end{bmatrix} \quad (14)$$

and

$$\begin{aligned} h &= r + e \\ &= f\begin{bmatrix} R(t_0) \\ R(t_1) \\ \vdots \\ R(t_C) \\ 0 \\ 0 \\ \vdots \\ 0 \end{bmatrix} + K_a \begin{bmatrix} 0 \\ 0 \\ \vdots \\ 0 \\ 1 \\ \exp(-K^{trans}\Delta t/v_e) \\ \vdots \\ \exp(-K^{trans}(N-1)\Delta t/v_e) \end{bmatrix} \\ &= \begin{bmatrix} H(t_0) \\ H(t_1) \\ \vdots \\ \vdots \\ \\ \\ \vdots \\ H(t_{N-1}) \end{bmatrix} \end{aligned} \quad (15)$$

where Δt is the sampling interval, N the number of data points, t_c the time index corresponding to T_c, $\Delta R2_t^*$ the apparent change in $R2^*$ in the tissue in the presence of T_1 effects and extravasation (equation (11)), and $\Delta R2_a^*$ the corresponding change in $R2^*$ in blood. Thus, equation (12) can be solved for $\mathbf{h}$ using standard matrix inversion methods such as singular value decomposition (SVD) (Ostergaard *et al*, 1996), and K_a is then approximated from the tail of $H(t)$ following the assumptions leading up to equation (9).

The apparent blood volume measured in a leaky voxel is given by the area under $H(t)$, which can be expressed in terms of the intravascular (v_i) and extracellular (v_e) volume fractions as follows:

$$\begin{aligned} v_T &\approx f\int_0^{T_c} R(t)dt + K_a \\ &\quad \times \int_{T_c}^{\infty} \exp(-K^{trans}(t-T_c)/v_e)dt \\ &= v_i + v_e \end{aligned} \tag{16}$$

The intravascular blood volume (in units of mL blood/100 g) is then given by:

$$CBV_i = \frac{H_c}{\rho}(v_T - v_e) \tag{17}$$

As we have assumed negligible CA reflux within the total sampling time, v_e cannot be estimated but the error in CBV_i caused by CA extravasation can then be estimated from the approximation $H(t) \approx K_a$ for $t >> T_c$, so that the leakage-corrected intravascular blood volume is given by:

$$\begin{aligned} &CBV_{corr} = CBV_{app} - K_a \Delta t(N - N_c)/\rho; \\ &N\Delta t K^{trans}/v_e << 1, \end{aligned} \tag{18}$$

where CBV_{app} is the apparent CBV value measured by equation (5) and N_c the time index corresponding to T_c. Here, T_c is unknown and tissue dependent, but may be estimated by fitting the initial portion of $H(t)$ to an appropriate parametric function. Cerebral blood flow is not affected by CA extravasation effects because $H(t) = fR(t)$ $(t << T_c)$ is not dependent on K_a.

Materials and methods

Patient Material

Study approval was obtained from the Regional Medical Ethics Committee, and patients were included only if informed consent was obtained. A total of 101 patients (51 males, mean age 51 years, range 8 to 79 years) with confirmed glioma, selected from an ongoing prospective tumor perfusion study were included in the analysis. The histopathological diagnosis of the included patients is specified in a previous study (Bjornerud and Emblem, 2010), and for this study, patients were divided into two groups in which glioma grades I and II were grouped as low-grade gliomas (LGGs) and glioma grades III and IV were grouped as high-grade gliomas (HGGs).

Magnetic Resonance Imaging

Imaging was performed at 1.5 Tesla (Siemens Sonata, Symphony or Avanto, Siemens AG, Erlangen, Germany), using an 8-channel (Symphony/Sonata) or a 12-channel (Avanto) head-coil. Dynamic susceptibility contrast-MRI was performed using a GRE-EPI sequence acquired during CA administration. The DSC imaging parameters were: repetition time (TR)/TE/flip angle 1,430 milliseconds/46 milliseconds/90°, bandwidth 1,345 Hz/pixel (12 axial slices) or 1720/48/90, bandwidth 1,500 Hz/pixel (14 axial slices), field of view $230 \times 230\,mm^2$, voxel size $1.8 \times 1.8 \times 5\,mm^3$, interslice gap 1.5 mm. For each slice, 70 images were recorded at intervals equal to the TR. After eight time points, 0.2 mmol/kg of the CA gadobutrol (Gadovist, Bayer Schering Pharma AG, Berlin, Germany) was injected at a rate of 5 mL/sec, immediately followed by a 20 mL bolus of saline (B. Braun Melsungen AG, Melsungen, Germany), also at 5 mL/sec. The image protocol included axial T_2-weighted fast spin-echo images (TR/TE = 4,000 milliseconds/104 milliseconds), coronal fluid-attenuated inversion recovery images (TR/TE = 9,050 milliseconds/114 milliseconds and inversion time (TI) = 1,500 milliseconds) and axial T_1-weighted SE images (TR/TE = 500 milliseconds/7.7 milliseconds) obtained before and after intravenous CA injection. The voxel size was $0.45 \times 0.45 \times 5\,mm^3$ with 19 slices for the T_2- and T_1-weighted images and $0.9 \times 0.9 \times 5\,mm^3$ with 25 slices for the fluid-attenuated inversion recovery images.

Data Analysis

Perfusion Analysis and Extravasation Correction: The proposed extravasation-correction methods were compared with the reference method of Boxerman *et al* (2006), hereby referred to as Method I. Different from the original implementation, the constant K_2 (equation (1)) was allowed to assume both positive and negative values to account for the possible presence of both T_1- and T_2^*-dominant relaxation effects during CA extravasation. In the proposed alternative method (denoted Method II), the apparent transfer constant K_a was determined directly from the tail of the residue function as outlined in the 'Theory' section. Method I was used only to correct rCBV values normalized to the unaffected white matter (Emblem and Bjornerud, 2009), whereas Method II provided absolute estimates of cerebral blood flow (CBF) and leakage-corrected CBV and MTT from the residue function. The residue function was determined on a pixel-by-pixel basis (or from simulated response curves) using iterative Tikhonov-regularized SVD deconvolution (Bjornerud and Emblem, 2010). The intravascular residue function $R(t)$ was estimated by fitting the initial portion (first five time points) of $H(t)$ to a Lorentzian function of the form

(Calamante *et al*, 2003):

$$R(t) = \left[1 + \left(\frac{\pi \cdot t}{2T_c}\right)^2\right]^{-1} \quad (19)$$

where T_c is the intravascular transit time which was then used as an estimate of the cutoff point between the intravascular phase and the extravasation phase (equation (8)). The curve fit was performed using a Levenberg–Marquardt nonlinear least squares fitting procedure (Press *et al*, 1992). The Lorentzian function provided excellent goodness of fit to actual residue functions obtained in the unaffected white and gray matter (data not shown).

Simulations: Simulations were performed to investigate the validity of the two extravasation-correction methods under different hemodynamic conditions and to assess the sensitivity of the models to variations in underlying tissue relaxation properties and sequence parameters. For all simulations, the AIF was modeled as a γ-variate function (Benner *et al*, 1997), but with an additional exponential term to model steady-state effects:

$$\begin{aligned} \mathrm{Ca}(t) &= (t - T_0)^a \exp\left(-\frac{t - T_0}{b}\right) \\ &\quad + \mathrm{Ca_{ss}}\left(1 - \exp\left(-\frac{t - T_{0ss}}{\beta}\right)\right)\exp\left(-\frac{t - T_{0ss}}{T_{el}}\right) \end{aligned} \quad (20)$$

where a, b, β are curve-shape constants, T_0 the CA arrival time, T_{0ss} a time delay constant for the steady-state effect, $\mathrm{Ca_{ss}}$ the steady-state CA concentration, and $\mathrm{T_{el}}$ the plasma elimination half-life of the CA. The constants were chosen such that $\mathrm{Ca_{max}} = 7$ mmol/L and $\mathrm{Ca_{ss}} = 1$ mmol/L. A Lorentzian intravascular residue function (equation (19)) was used for all simulations.

Dependence of K_a on Transverse Relaxivity and Sequence Parameters: The concentration time curves $C_{t\_iv}(t)$ and $C_{t\_ev}(t)$ were estimated from the AIF by convolution (equations (3 and 6)) for given values of MTT, CBF, K^{trans}, and v_e, and the corresponding relaxation rate changes in the respective compartments were calculated as described below. Signal changes corresponding to the estimated CA-induced relaxation rate changes were then calculated using the expression for steady-state GRE signal behavior (equation (11)), and the corresponding changes in apparent $R2^*$ relaxation rates were calculated from the simulated signal changes, assuming negligible T_1 effects:

$$\Delta R2^*_{app}(C) = \frac{1}{TE}\ln\left(\frac{SI(0)}{SI(C)}\right) \quad (21)$$

$R2^*_{app}$ in tissue was then deconvolved with the AIF $R2^*$ response curve to estimate the residue function measured in the presence of extravasation and tissue relaxation effects. Finally, K_a was extracted from the residue function using Method II as described in the 'Theory' section.

Tissue T_1 and T_2^* relaxation rates were estimated by assuming linear dose-response functions:

$$\begin{aligned} R2^*(C) &= R2^*(0) + r2 \cdot C \\ R1(C) &= R1(0) + r1 \cdot C \end{aligned} \quad (22)$$

where $r1$ and $r2$ are the T_1 and T_2^* CA relaxivities, respectively, in a given tissue compartment, and $R1(0)$ and $R2^*(0)$ the relaxation rates in the absence of CA. Change in tissue T_1 relaxation was assumed to be a function of extravascular CA concentration only, assuming the intravascular T_1 relaxation contribution in tissue to be negligible. The CA-induced change in $R2^*$ relaxation rates was assumed to be a linear combination of the intravascular and extravascular contributions:

$$\Delta R2^*_t(C_{ev}, C_{iv}) = \Delta R2^*_{ev}(C_{ev}) + \Delta R2^*_{iv}(|C_{iv} - C_{ev}|) \quad (23)$$

The dependence of $\Delta R2^*_{iv}$ on $\Delta C = |C_{iv} - C_{ev}|$ is because of the fact that $\Delta R2^*_{iv}$ is proportional to the susceptibility difference ($\Delta\chi$) between the two compartments and $\Delta\chi \propto \Delta C$ (Kjolby *et al*, 2006). The effect of variations in extravascular structure and volume was simulated by varying the effective transverse relaxivity, $r2_{ev}$ in the EES. The value of $r2_{ev}$ was initially set equal to the dipolar value as obtained in a completely homogeneous solution ($r2 = 5.3$ L/mmol per sec) (Bleeker *et al*, 2009). This was assumed to be the lower limit in tissue with complete loss of cellular integrity. In tissues with intact cell membranes, $r2_{ev}$ will be higher because of field perturbations at the intracellular and extracellular interface. The effect of increasing the degree of compartmentalization was simulated by a step-wise increasing of $r2_{ev}$ up to a maximum value of 30 L/mmol per sec. For intravascular contribution, $r2_{iv} = 44$ L/mmol per sec was used, a value which was previously found to be valid for both gray and white matter in the brain at 1.5 T (Kjolby *et al*, 2006).

A linear dose response was also assumed for the AIF. Although studies have shown that $R2^*$ relaxation in large arteries is quadratically dependent on CA concentration, the automated AIF determination implemented in this study tends to select voxels located outside the large arteries where a linear $R2^*$ dose response and absence of T_1 relaxation effects can be assumed (Bleeker *et al*, 2009). The tissue contribution to the AIF was assumed to be negligible, and an arterial $R2^*$ relaxivity $r2_a$ of 8 L/mmol per sec was used. The value of $r2_a$ was considered being close to the linear component of the intravascular relaxivity previously described, a value which was also found to give AIF $R2^*$ response curves in good agreement with results in patient data. For T_1 relaxivity in the EES, $r1 = 4.2$ L/mmol per sec was used.

K_a estimated from the above method was compared with the actual K^{trans} over a relevant range of K^{trans} (corresponding to extraction fractions $0 \leqslant E \leqslant 0.5$, where $E = K^{trans}/f$). Sequence parameters were kept constant except for the flip angle that was varied between 30° and 90°. The effect of using a predose was also simulated by estimation of the respective CA concentrations in all compartments after a first injection, and using these concentration values as baseline values for a second injection. The following additional parameters were fixed for all simulations: TR/TE = 1,500 milliseconds/45 milliseconds, CBF = 80 mL/100 g per min, and MTT = 5 seconds.

Mean Transit Time Dependence: Using predefined values of CBF, MTT and K_a tissue response curves were generated according to equations 13 to 15. Gaussian noise corresponding to an signal-noise ratio (SNR) of 50 in the raw data was added. Defining the apparent extraction fraction as $E_a = K_a/f$, simulations were performed with $E_a = 0.1$ and

$E_a = -0.1$ to model both T_1- ($E_a < 0$) and T_2^*- ($E_a > 0$) dominant extravasation effects. The simulated leakage-affected response curves were then used to estimate K_a or K_2, and the corresponding leakage-corrected perfusion metrics obtained using the two correction methods were compared with the same values in the absence of extravasation. When applying correction Method I to the simulated data, a reference tissue response curve with $E_a = 0$, MTT = 5 seconds, and CBF = 40 mL/100g per min was assumed and leakage-corrected response curves were generated from equation (1). When varying MTT, CBF was kept constant at 80 mL/100g per min, so that CBV varied as a function of MTT. Finally, in the case of no extravasation, MTT varied between 0.5 and 4 times the corresponding MTT in the reference tissue ($0.5 <$ normalized MTT (nMTT) < 4). For a given nMTT, the error in K_2 (i.e., deviation from zero) and the corresponding error in the leakage-corrected rCBV value were estimated. The error in rCBV was estimated as the percentage difference between rCBV values obtained when applying leakage correction according to Method I compared with values obtained without applying leakage correction.

All data simulations were performed in Matlab 2007a (MathWorks, Natick, MA, USA).

Comparison of Extravasation-Correction Methods in Patient Data: The sensitivity of correction Method I to variations in MTT was tested based on pixel-wise analysis in selected tumors (with tumor MTT values deviating from MTT in nonpathologic tissues) and compared with the expected results based on the simulations. Leakage-corrected MTT values (obtained using correction Method II) were extracted from each voxel within the tumor region of interest and normalized to the MTT derived from a mask of unaffected white and gray matter to yield nMTT values, which were correlated with the corresponding pixel-wise K_2 and K_a values. To estimate the error in K_2 as a function of nMTT, K_a was assumed to be linearly related to K_2 for values of nMTT close to unity. Selecting only tumor pixels with nMTT ≈ 1, the linear correlation coefficient was then estimated so that $K_2^{est} = \alpha K_a$. Under the assumption that K_a is independent of nMTT, the error in K_2 as a function of nMTT was then $\Delta K_2 = \alpha K_a - K_2$. The same tissue mask used to extract normalized MTT values was used to determine the reference tissue response curve when estimating K_2 according to Method I (equation (1)), so that for pixels with nMTT ≈ 1, it would be expected that $\Delta K_2 \approx 0$. Finally, under the assumption that corrected CBV obtained from Method II (CBV(II)) is independent of nMTT, the percentage difference between CBV(II) normalized to unaffected white matter and normalized CBV (nCBV) (I) was plotted as a function of nMTT.

Tumor Segmentation: Using anatomic MR images, binary glioma regions of interest were derived from each MR image slice using an automatic tumor segmentation routine based on knowledge-based Fuzzy c-means clustering (Emblem *et al*, 2009).

Parametric Image Generation: Applying the two correction methods, parametric leakage maps were generated in which T_1- and T_2^*-dominant leakage constants (K_2, Method I or K_a, Method II) were rendered with different color palettes (blue for positive T_2^*-dominant leakage and red for negative T_1-dominant leakage). Positive and negative K_2 and K_a values were identified in the segmented tumor volume and analyzed separately. When differentiating T_1- and T_2^*-dominant leakage effects, the transfer constants are referred to as $K_a(T_1)$ and $K_a(T_2^*)$, respectively, for T_1- and T_2^*-dominant effects.

All image-processing methods, except for the tumor segmentation method were performed using a modified version of nordicICE (NordicImagingLab AS, Bergen, Norway). Tumor segmentation was performed in Matlab R2007a.

Statistical Comparisons

Group differences between HGGs and LGGs for the derived hemodynamic parameters were tested using the Mann–Whitney *U*-test with a significance level of 0.01. Using normalized histogram peak values derived from the corrected CBV values from tumor segments (Emblem *et al*, 2008), logistic regression was used in combination with available survival data to derive Kaplan–Meier survival curves with regard to separating a 'high-risk group' (survival $<$ 1year after MRI exam) from a 'low-risk group' (survival $>$ 1year) regardless of histopathological grading. Statistical analysis was performed using SPSS 17 (SPSS Inc., Chicago, IL, USA).

Results

Simulations

Figure 1 shows the results of the simulation of the correlation between K_a and K^{trans} as function of flip angle (panel A), extravascular transverse relaxivity ($r2_{ev}$) (panel B), and the presence or absence of predose (panel C). K_a was generally found to be a nonlinear function of K^{trans}. At low values of K^{trans} and $r2_{ev}$, combined with large flip angles, K_a was initially negatively related to K^{trans} because of a T_1-dominant leakage effect. At higher K^{trans} values, K_a was almost independent of K^{trans} for low values of $r2_{ev}$. With increasing $r2_{ev}$ and reduction in flip angle, K_a became increasingly positive (T_2^*-dominant leakage) and was a positive function of K^{trans}. The use of predose resulted in mainly T_2^*-dominant leakage effects and, except for an initial negative dip, K_a being a positive function of K^{trans} even for high flip angles and low $r2_{ev}$ values.

Figure 2 shows the correlations between the estimated CBV and MTT after extravasation correction using the two correction methods compared with actual and uncorrected values. Method II was able to reproduce the reference values after correction for both perfusion metrics, whereas Method I resulted in an increasing underestimation of CBV and MTT with increasing MTT and CBV values. Uncorrected CBV and MTT values were significantly

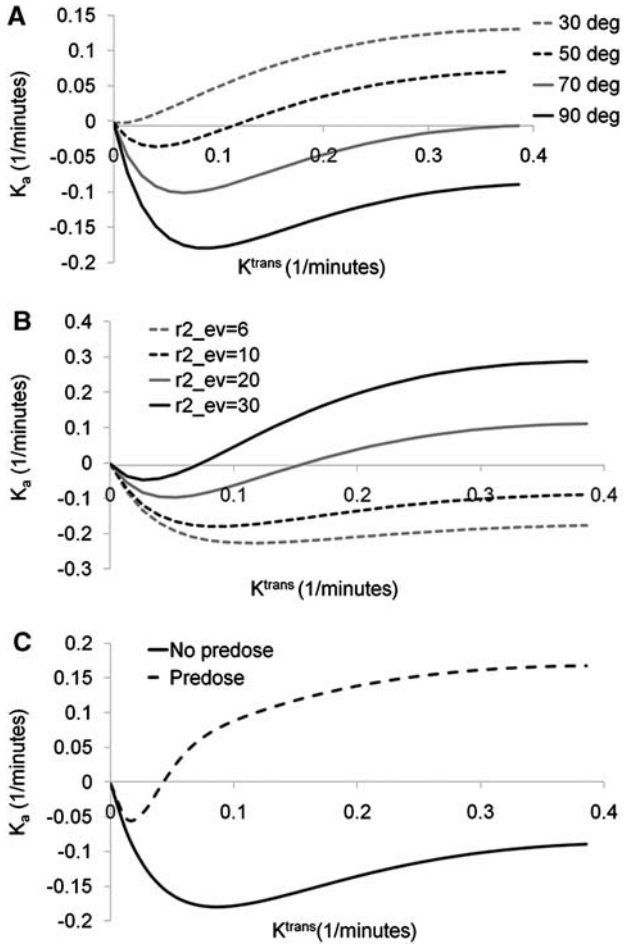

Figure 1 Simulations of the relationship between the apparent transfer constant (K_a) and K^{trans}. The relationship is shown as function of (**A**) flip angle, (**B**) effective transverse relaxivity (in units of L/mmol per sec) in the EES, and (**C**) presence or absence of pre-dose. In panels **A** and **C**, a value of $r2_{ev} = 20$ L/mmol per sec was used and for panels **B** and **C**, a flip angle of 90° was used.

overestimated for T_2^*-dominant leakage and underestimated for T_1-dominant leakage. Cerebral blood flow was not significantly affected by extravasation effects (data not shown).

Figure 3 shows the simulated error in K_2 (ΔK_2) as a function of nMTT (panel A) and the corresponding error in rCBV (ΔrCBV) in percentage after correction using Method I (panel B) in the situation of no CA extravasation ($E = 0$). ΔK_2 increased quadratically with increasing nMTT and nMTT >1 resulted in a linear increase in the relative underestimation in rCBV because of an artificially positive value of K_2. The error for nMTT <1 was small for both rCBV and K_2.

Patient Data

Approximately 60% of all tumors with detectable CA extravasation exhibited predominantly T_1-enhancing leakage effects (defined as $>70\%$ of tumor voxels with nonzero K_a having $K_a < 0$). Approximately 10% of tumors exhibited predominantly T_2^*-enhancing leakage, and the remaining 30% had an approximately equal mix of T_1- and T_2^*- dominant leakage effects. Figure 4A shows two glioblastoma cases showing T_1-dominant (left) and T_2^*-dominant extravasation effects. Figure 4B shows the corresponding dose-response curves and residue functions for the same two sample cases. As predicted by theory and simulations, the T_1-dominant leakage resulted in a negative tail in the residue function and T_2^*-dominant leakage resulted in a positive tail.

Two selected sample cases showing the effect of elevated tumor MTT values are shown in Figure 5. The top row shows a grade III anaplastic astrocytoma with significant elevation of nMTT in tumor resulting in apparent T_2^*-dominant leakage as seen in the K_2 map in spite of the absence of visible contrast enhancement in the T_1-weighted image after CA administration. The artificial T_2^*-dominant leakage resulted in lower nCBV in tumor compared with CBV obtained with Method II. The bottom row shows a glioblastoma with elevated MTT values in the tumor rim resulting in overestimation of K_2 and in underestimation of nCBV in areas of elevated MTT values.

Figure 6 shows pixel-wise analysis of error in K_2 and rCBV as function of nMTT for two cases selected based on the presence of a large range of nMTT values in tumor. The left column shows the correlation between K_a and K_2 for all pixels with $0.9 <$ nMTT < 1.1. A significant and similar linear correlation was observed between K_a and K_2 for voxels with nMTT ≈ 1 in both cases, and the regression coefficients could therefore be used to determine the residual error in K_2 as a function of nMTT. Both cases showed an increase in ΔK_2 (center column) and a negative increase in percentage difference between nCBV(I) and nCBV(II) (right column) with increasing nMTT. ΔK_2 had zero crossing at about nMTT $= 1$, in good agreement with simulations (Figure 3).

The mean leakage-corrected whole-tumor CBV ($\pm$ s.d.) was 2.1 ± 0.8 mL/100 g and 3.9 ± 1.7 mL/100 g in LGGs and HGGs, respectively ($P < .001$). Using the same correction method, both mean MTT and $K_a(T_2^*)$ were significantly higher ($P < .001$) in HGGs than in LGGs. The average MTT in HGG was 5.6 ± 1.5 seconds and 4.0 ± 1.0 seconds in LGGs. Mean $K_a(T_2^*)$ was 0.17 ± 0.08 per min in HGGs and 0.11 ± 0.08 per min in LGGs. $K_a(T_1)$ was not significantly different in HGGs and LGGs. The K_a values obtained *in vivo* were in the same range as those obtained in the simulations (Figure 1). For the Kaplan–Meier analysis, the log-rank (Mantel–Cox χ^2) values describing the difference between the low- and high-risk survival curves were higher for correction Method II than for Method I (23.69; $P < .001$ and 16.46; $P < .001$, respectively). The Kaplan–Meier survival curves are shown in Figure 7.

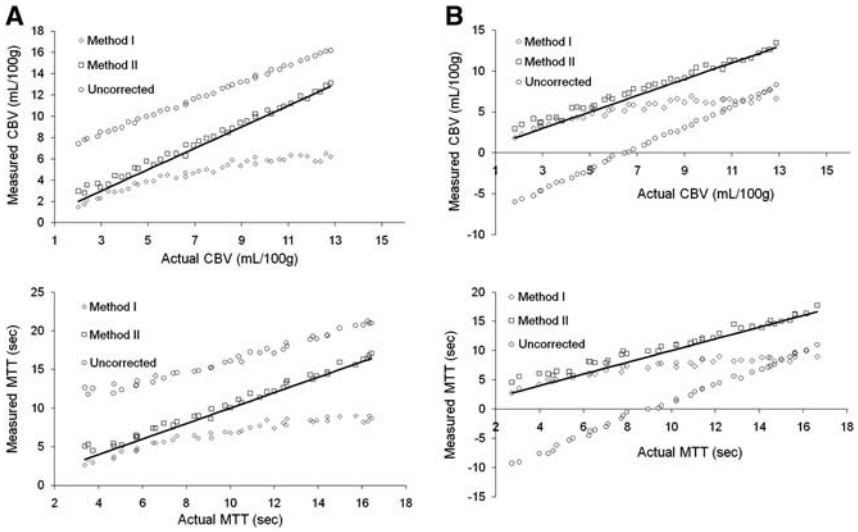

Figure 2 Simulations of the sensitivity of the two leakage correction methods to variations in the underlying hemodynamics and CA extravasation properties. The solid lines indicate the line of unity. The results are shown for (**A**) T_2^*-dominant extravasation (E_a=0.1) and (**B**) T_1-dominant extravasation (E_a=−0.1). In both cases, correction Method II enabled good reproduction of the actual hemodynamic parameters independent of the underlying values of CBV and MTT. Method I resulted in under-estimation of CBV and MTT at high MTT and CBV values. Uncorrected CBV and MTT were over-estimated for T_2^*-dominant leakage and under-estimated for T_1-dominant extravasation effects. CBV, cerebral blood volume; MTT, mean transit time.

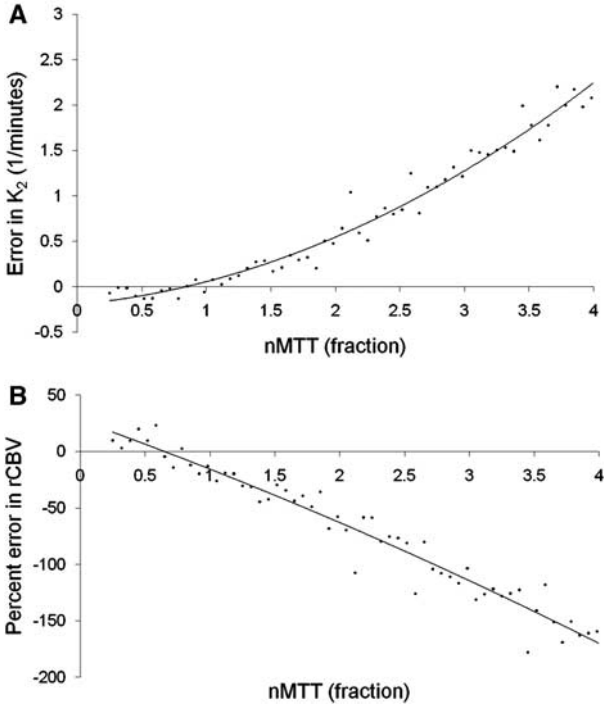

Figure 3 Simulation of errors in K_2 due to MTT effects.Simulated error in (**A**) K_2 and (**B**) percentage error in corrected rCBV values (using Method I) as a function of normalized MTT (nMTT). nMTT represents the ratio of MTT between tumor and reference tissue. The simulations were performed with nominal zero extravasation ($E = 0$) so that the Y axis in (**A**) reflects the actual error in K_2 as a function of nMTT. rCBV, relative cerebral blood volume.

Discussion

In this study, we introduce a novel method which enables estimation of CA extravasation and multiple perfusion metrics directly from the tissue residue function. This development was motivated by limitations in existing methodology and an identified need for quantitative assessment of tumor hemodynamic properties. Although a postprocessing-based method for leakage correction is established (Boxerman *et al*, 2006), two important limitations of this reference-correction method were identified: (1) the method is sensitive to deviations in tumor MTT compared with reference tissue MTT and (2) the method only corrects for T_1-dominant leakage. The latter point can easily be overcome by allowing the apparent transfer constant (K_2) to assume both positive and negative values. However, MTT sensitivity is inherent in the method, and we show through simulations and in patient data that elevated MTT in tumor tissue may lead to underestimation of rCBV as a result of incorrect estimation of K_2. Given that MTT was found to be significantly higher in HGGs than in LGGs, our results suggest that the reference method may underestimate rCBV in tumors even when leakage correction is performed. The proposed correction method providing absolute leakage-corrected CBV values was found to provide improved survival prediction compared with the reference-correction method of Boxerman *et al* applied to normalized CBV values. The survival

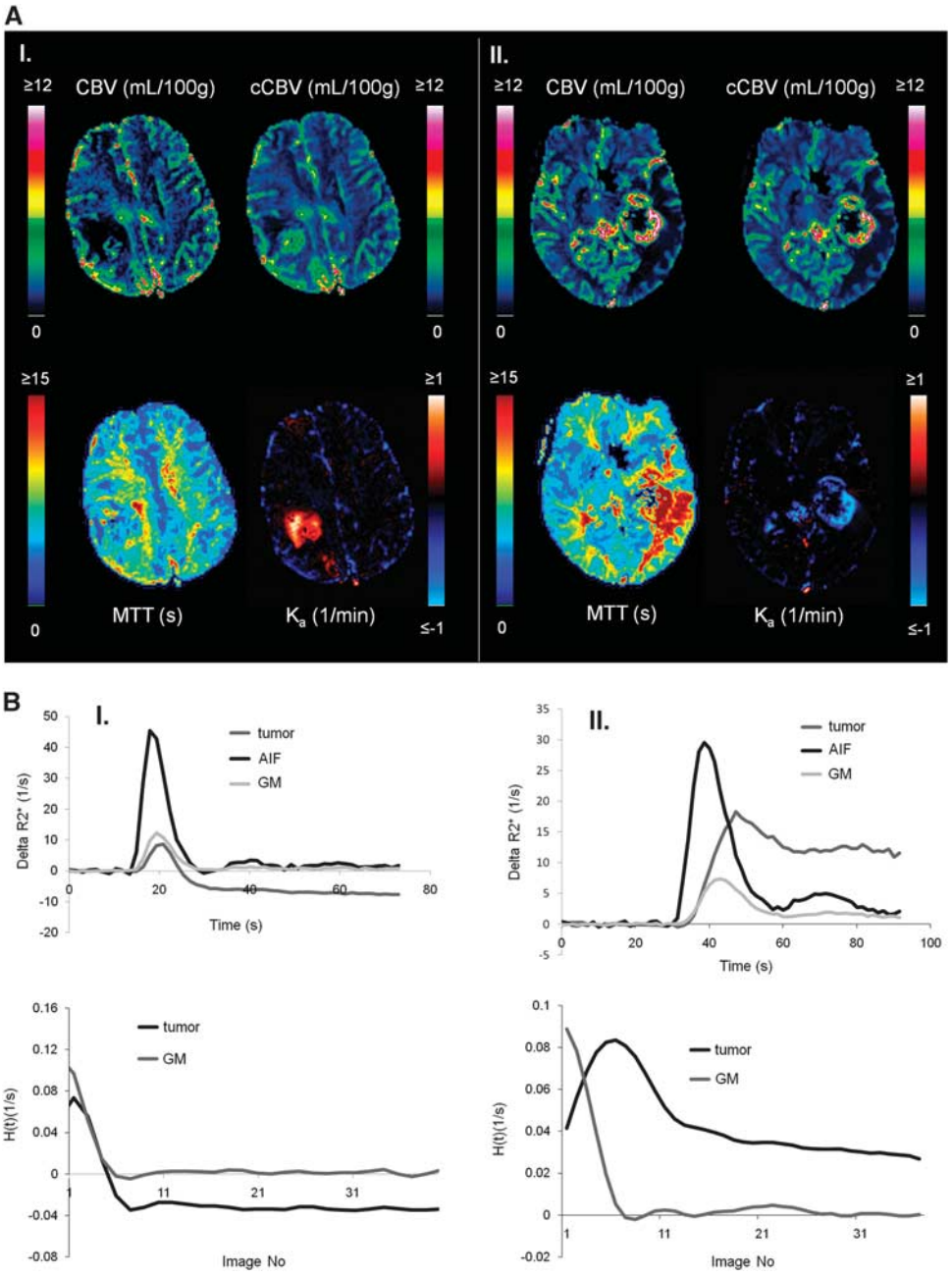

Figure 4 Sample cases showing T_1- and T_2^*-dominant CA extravasation analyzed using Method II. (**A**) The images show non-corrected (CBV) and leakage-corrected (cCBV) cerebral blood volume maps, leakage-corrected MTT maps and apparent rate constant (K_a) maps where blue-shade colors represent T_2^*-dominant K_a values and red-shade colors T_1-dominant K_a values. In spite of same tumor grade, sequence parameters, and contrast agent dose, case I (left, male 40 years) exhibits predominant T_1-extravasation, whereas case II (right, male 60 years) exhibits predominant T_2^*-extravasation. (**B**) Dose-response curves (top row) and corresponding residue functions obtained from tumor ROIs from the cases shown in panel **A**. CBV, cerebral blood volume; MTT, mean transit time; ROI, region of interest.

analysis was based on whole-tumor CBV histogram analysis (Emblem *et al*, 2008), an approach previously shown to robustly predict outcome from automatically generated tumor regions of interest (Emblem *et al*, 2009).

The problem of MTT sensitivity of the reference method has previously been pointed out by other investigators. Quarles *et al* (2005)proposed an alternative MTT-insensitive correction method which also relies on AIF deconvolution. Different from the method of Quarles *et al*, we aimed at estimating all hemodynamic parameters directly from the leakage-corrected tissue residue function, thereby avoiding the step of regenerating a leakage-corrected tissue response curve. Although no gold standard currently exists, alternative models providing a combined

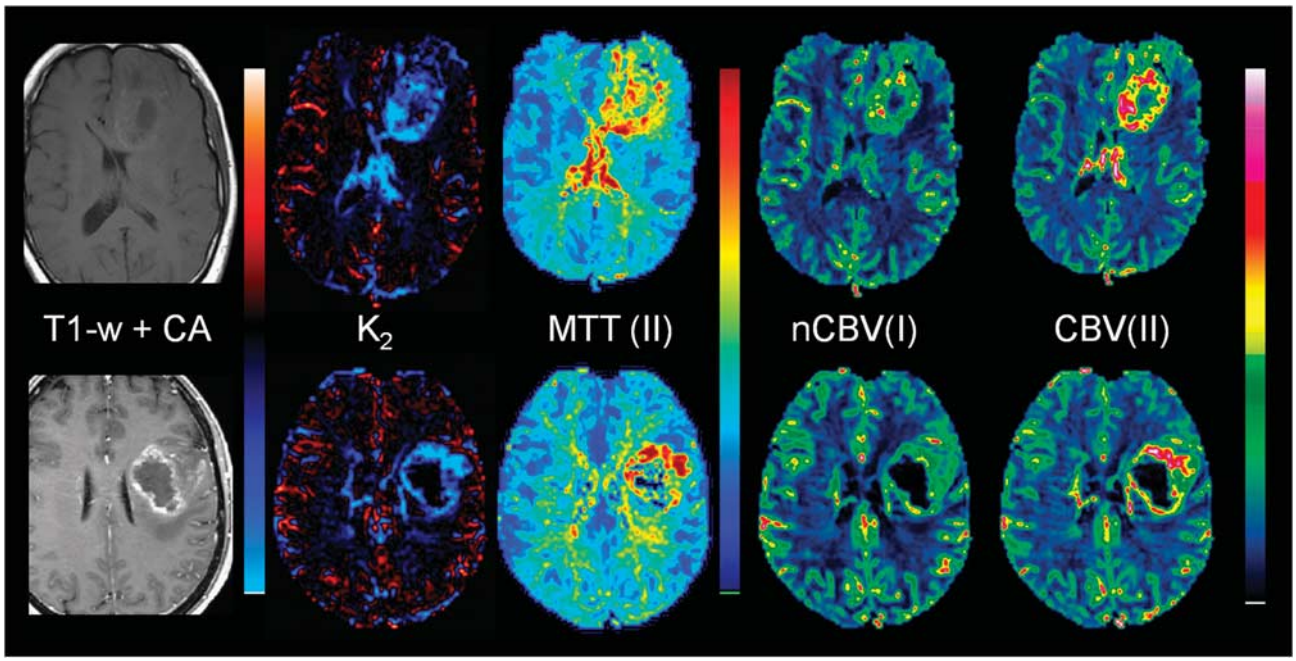

Figure 5 Sample cases showing leakage-correction error using Method I owing to significant deviations in MTT between reference tissue and tumor. The top row shows results in a patient with grade III anaplastic astrocytoma (male, age 53 years). The tumor exhibits significantly elevated MTT values, resulting in large T_2^*-dominant leakage effects in the tumor in spite of the absence of contrast enhancement on the postcontrast T_1-weighted image. The incorrect $K_2(T_2^*)$ estimation results in underestimation of nCBV using Method I (nCBV(I)) compared with the results of Method II (CBV(II)). The bottom row shows results in a patient glioblastoma (female, age 56 years). A similar overestimation of K_2 is observed in areas of elevated MTT, with corresponding underestimation of nCBV in the same regions as compared with the CBV values obtained with Method II. nCBV, normalized cerebral blood volume; MTT, mean transit time.

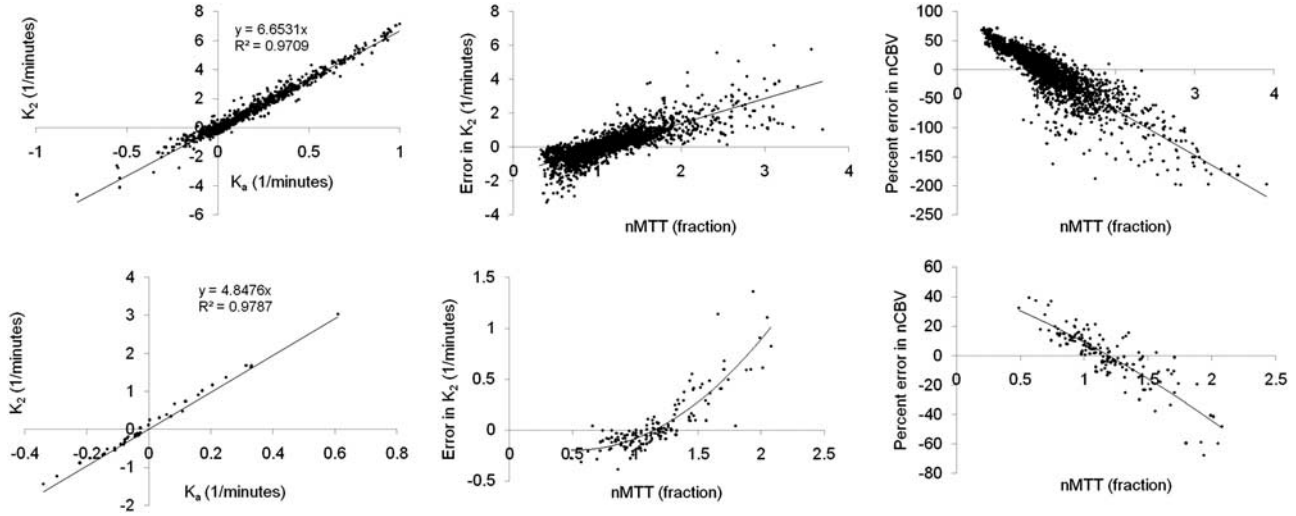

Figure 6 Pixel-wise analysis of error in K_2 and nCBV as function of nMTT in two sample cases. The left column shows the relationship between K_a and K_2 for pixels with $0.9 < \text{nMTT} < 1.1$. A high correlation was observed in both cases confirming the validity of the assumption that K_a and K_2 are linearly related for nMTT values close to unity. The middle column shows the deviation (ΔK_2) from the expected linear relationship between K_2 and K_a as function of nMTT. The right column shows the percentage deviation between normalized corrected CBV values (nCBV) obtained with Method I and nCBV values obtained with Method II (ΔnCBV) as function of nMTT. The resulting dependence of ΔK_2 and ΔnCBV on nMTT was found to be in good agreement with results from simulations as shown in Figure 3. nMTT, normalized mean transit time; nCBV, normalized cerebral blood volume.

assessment of both perfusion and CA extravasation have been proposed (Larsson *et al*, 2009; Singh *et al*, 2007). The approach of Larsson *et al* is similar to that of ours in that it is based on a model-independent estimation of the leakage-affected residue function using Tikhonov-regularized deconvolution. However, they estimated the perfusion and permeability parameters by fitting the obtained residue function to

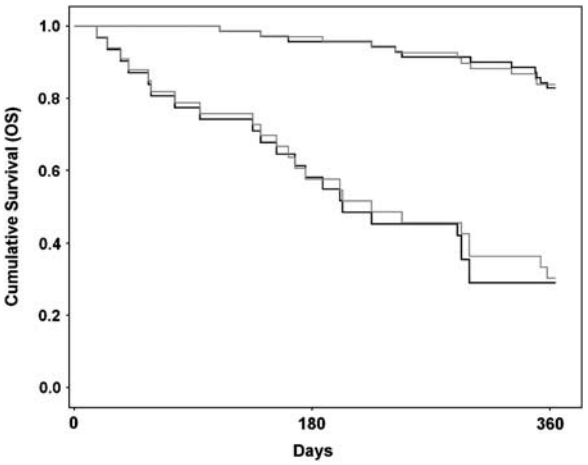

Figure 7 Kaplan–Meier survival analysis for Method II (black lines) compared with Method I (gray lines) when separating a 'high-risk' group with expected survival of < 1 year from a 'low-risk' group with expected survival of > 1 year. A higher log-rank value was observed for correction Method II than for Method I (23.69 versus 16.46).

a comprehensive two-compartment model. Their approach was found to give robust estimates of both perfusion and permeability when applied to T_1-weighted dynamic contrast-enhanced MRI. It remains an open question what the added value of such complex models may be when applied to DSC-MRI because of a much less predictable dose response in tumor tissue with this acquisition method, as shown in our study.

The model assumptions used in the presented correction method deviates somewhat from our previously proposed model in which capillary perfusion and extravascular leakage were assumed to occur as two parallel processes originating from the same arterial source (Bjornerud and Emblem, 2009). Although the current model probably better describes the underlying kinetics of the CA, the estimation of K_a is in practice identical for the two models and the CBV correction differs only by the nonzero offset value N_c (equation (18)) in the modified model.

In spite of eliminated MTT sensitivity in relation to CA leakage estimation, the proposed method has limitations. It is known that SVD-based deconvolution may underestimate flow values when MTT becomes too short relative to the sampling rate (Wu *et al*, 2003). This effect could lead to a bias in the estimated MTT values. However, we did find MTT to be significantly increased in HGGs than in LGGs, suggesting that CBV increases relatively more than does CBF in malignant gliomas. It is therefore believed that MTT errors owing to limited sampling rate may not be significant in this patient population, but this assumption needs to be investigated further. Moreover, the proposed method relies on accurate estimation of the tissue residue function, which requires both robust estimation of the AIF and stable deconvolution in the presence of noise. Given the recent advent of automated AIF detection methods (Carroll *et al*, 2003; Mouridsen *et al*, 2006), it is expected that much of the current user dependence associated with AIF determination can be eliminated. The need of the method to identify a 'steady-state' level in a noisy and generally oscillating residue function is also a challenge. We minimized oscillations by using an iterative Tikhonov regularization-based SVD deconvolution method (Calamante *et al*, 2003; Hansen and Oleary, 1993) and were able to obtain robust estimates of both T_1- and T_2^*-dominant leakage effects using this approach.

Computer simulations were used to investigate the relationship between the measured apparent rate constant K_a and K^{trans}. Although the performed simulations make several simplifying assumptions regarding *in vivo* relaxation effects, the results clearly suggest that the apparent transfer constant estimated from DSC-MRI is generally not linearly related to the underlying permeability surface area product (PS) of the tumor tissue, even when extravasation is permeability limited ($CBF >> PS$). This lack of linear correlation is partly attributed to the complex relationship between CA concentration in tissue and the measured change SI and corresponding transformation to apparent transverse relaxation rates. The presence of both T_1 and T_2^* relaxation effects in the EES can result in both positive and negative apparent rate constants depending on the underlying tissue properties, as well as sequence parameters. The presence of both these effect was confirmed in the patient data. An additional source of nonlinearity is attributed to the assumption of negligible CA reflux. For the higher K^{trans} values tested in these simulations, the required condition that $K^{trans}T_N/v_e << 1$ is clearly violated, resulting in an underestimation of K_a at high K^{trans} values. An improved model in which the tail of $H(t)$ is not assumed to be a constant but is fitted to the full exponential function (equation (15)) is therefore warranted and may provide a better estimate of K^{trans}. However, even with improved kinetic models, absolute estimations of K^{trans} from DSC acquisitions will remain challenging because of an unpredictable and generally nonlinear dose response in DSC-MRI.

The simulations confirmed that the use of a predose reduces T_1 effects and gives predominantly positive K_a values except at very low K^{trans}, in which an initial negative 'dip' was observed. The presence of this initial 'inverted' K_a response at low K^{trans} values could be a potential challenge but this effect needs to be confirmed in clinical data in which a predose is used. In this study, no predosing and a large flip angle of 90° was used, both factors resulting in an increased sensitivity to T_1-dominant leakage effects. Although K_a should be expected to correlate with tumor grade, such a correlation was only observed for $K_a(T_2^*)$. The lack of correlation of $K_a(T_1)$ with tumor grade may be because of the

nonlinear dependence, and to a certain degree the nondependence of $K_a(T_1)$ and $(K_a < 0)$ on K^{trans}, as seen in Figures 4A and 4B. Given the results of the simulations showing that transition from T_1- to T_2^*-dominant leakage depends strongly on the effective transverse relaxivity in the EES, it could be hypothesized that the presence or absence of the two competing leakage effects may convey relevant information regarding the extravascular tissue structure within the tumor. This effect could thus be a potential marker for assessment of treatment response by, for instance, monitoring of changes in the relative $K_a(T_1)/K_a(T_2^*)$ fraction during treatment. This observation warrants further investigation.

In summary, we present a novel extravasation-correction method which enables robust correction for both T_1- and T_2^*-dominant leakage effects independent of the MTT of the target tissue. The method was combined with automated methods for AIF detection, providing estimates of multiple hemodynamic parameters without user interaction. Given the recent focus on longitudinal image-based assessment of treatment response in brain tumor therapy, user-independent analysis methods will become increasingly important. To this end, the utility of the presented perfusion analysis methodology will be tested in longitudinal tumor treatment monitoring analysis in follow-up of this study.

Acknowledgements

The authors thank Inge Rasmussen MD, PhD, for critical reading of this manuscript.

Disclosure/conflict of interest

AB Consultant/Advisory Boards; NordicNeuroLab AS, Bergen, Norway. *KEE*: Grant support; Norwegian Research Council; 191088/V50. *AGS*: Grant support; National Cancer Institute, National Institutes of Health. Consultant/Advisory boards; ACR-Image Metrix, BayerScheringPharma, Bristol Meyers Squibb, BiogenIdec, Merrimack Pharmaceuticals, Olea Medical, Mitsubishi Pharma, GE Healthcare, Regeneron, Novartis, Roche, Siemens Medical, Takeda, AstraZeneca, National Institutes of Health, Kit, Inc. *KM*: No potential conflicts of interest.

References

Benner T, Heiland S, Erb G, Forsting M, Sartor K (1997) Accuracy of gamma-variate fits to concentration-time curves from dynamic susceptibility-contrast enhanced MRI: influence of time resolution, maximal signal drop and signal-to-noise. *Magn Reson Imaging* 15:307–17

Bjornerud A, Emblem KE (2009) Estimation of contrast agent extravasation from the tissue residue function: application to tumor perfusion imaging. In: *Proceedings of the 17th Annual Meeting of International Society of Magnetic Resonance in Medicine (ISMRM)*. Honolulu, USA

Bjornerud A, Emblem KE (2010) A fully automated method for quantitative cerebral hemodynamic analysis using DSC-MRI. *J Cereb Blood Flow Metab* 30:1066–78

Bleeker EJ, van Buchem MA, van Osch MJ (2009) Optimal location for arterial input function measurements near the middle cerebral artery in first-pass perfusion MRI. *J Cereb Blood Flow Metab* 29:840–52

Boxerman JL, Hamberg LM, Rosen BR, Weisskoff RM (1995) MR contrast due to intravascular magnetic susceptibility perturbations. *Magn Reson Med* 34:555–66

Boxerman JL, Schmainda KM, Weisskoff RM (2006) Relative cerebral blood volume maps corrected for contrast agent extravasation significantly correlate with glioma tumor grade, whereas uncorrected maps do not. *AJNR Am J Neuroradiol* 27:859–67

Calamante F, Gadian DG, Connelly A (2002) Quantification of perfusion using bolus tracking magnetic resonance imaging in stroke: assumptions, limitations, and potential implications for clinical use. *Stroke* 33:1146–51

Calamante F, Gadian DG, Connelly A (2003) Quantification of bolus-tracking MRI: improved characterization of the tissue residue function using Tikhonov regularization. *Magn Reson Med* 50:1237–47

Carroll TJ, Rowley HA, Haughton VM (2003) Automatic calculation of the arterial input function for cerebral perfusion imaging with MR imaging. *Radiology* 227: 593–600

Donahue KM, Krouwer HG, Rand SD, Pathak AP, Marszalkowski CS, Censky SC, Prost RW (2000) Utility of simultaneously acquired gradient-echo and spin-echo cerebral blood volume and morphology maps in brain tumor patients. *Magn Reson Med* 43:845–53

Donahue KM, Weisskoff RM, Burstein D (1997) Water diffusion and exchange as they influence contrast enhancement. *J Magn Reson Imaging* 7:102–10

Emblem KE, Bjornerud A (2009) An automatic procedure for normalization of cerebral blood volume maps in dynamic susceptibility contrast-based glioma imaging. *AJNR Am J Neuroradiol* 30:1929–32

Emblem KE, Nedregaard B, Hald JK, Nome T, Due-Tonnessen P, Bjornerud A (2009) Automatic glioma characterization from dynamic susceptibility contrast imaging: brain tumor segmentation using knowledge-based fuzzy clustering. *J Magn Reson Imaging* 30:1–10

Emblem KE, Nedregaard B, Nome T, Due-Tonnessen P, Hald JK, Scheie D, Borota OC, Cvancarova M, Bjornerud A (2008) Glioma grading by using histogram analysis of blood volume heterogeneity from MR-derived cerebral blood volume maps. *Radiology* 247:808–17

Hansen PC, Oleary DP (1993) The use of the L-curve in the regularization of discrete iii-posed problems. *Siam J Sci Comput* 14:1487–503

Kjolby BF, Ostergaard L, Kiselev VG (2006) Theoretical model of intravascular paramagnetic tracers effect on tissue relaxation. *Magn Reson Med* 56:187–97

Larsson HB, Courivaud F, Rostrup E, Hansen AE (2009) Measurement of brain perfusion, blood volume, and blood-brain barrier permeability, using dynamic contrast-enhanced T(1)-weighted MRI at 3 Tesla. *Magn Reson Med* 62:1270–81

Larsson HB, Stubgaard M, Frederiksen JL, Jensen M, Henriksen O, Paulson OB (1990) Quantitation of blood-brain barrier defect by magnetic resonance imaging and gadolinium-DTPA in patients with multiple sclerosis and brain tumors. *Magn Reson Med* 16:117–31

Lassen N, Perl W (1979) *Tracer Kinetic Methods in Medical Biology*. New York, NY: Raven Press

Lev MH, Rosen BR (1999) Clinical applications of intracranial perfusion MR imaging. *Neuroimaging Clin N Am* 9:309–31

Mouridsen K, Christensen S, Gyldensted L, Ostergaard L (2006) Automatic selection of arterial input function using cluster analysis. *Magn Reson Med* 55:524–31

Ostergaard L, Weisskoff RM, Chesler DA, Gyldensted C, Rosen BR (1996) High resolution measurement of cerebral blood flow using intravascular tracer bolus passages. Part I: mathematical approach and statistical analysis. *Magn Reson Med* 36:715–25

Paulson ES, Schmainda KM (2008) Comparison of dynamic susceptibility-weighted contrast-enhanced MR methods: recommendations for measuring relative cerebral blood volume in brain tumors. *Radiology* 249:601–13

Press WH, Teukolski SA, Vetterling WT, Flannery BP (1992) *Numerical Recipes in C. The Art of Scientific Computing*. Cambridge: Cambridge University Press pp 681–8

Quarles CC, Ward BD, Schmainda KM (2005) Improving the reliability of obtaining tumor hemodynamic parameters in the presence of contrast agent extravasation. *Magn Reson Med* 53:1307–16

Rempp KA, Brix G, Wenz F, Becker CR, Guckel F, Lorenz WJ (1994) Quantification of regional cerebral blood flow and volume with dynamic susceptibility contrast-enhanced MR imaging. *Radiology* 193:637–41

Rosen BR, Belliveau JW, Vevea JM, Brady TJ (1990) Perfusion imaging with NMR contrast agents. *Magn Reson Med* 14:249–65

Singh A, Haris M, Rathore D, Purwar A, Sarma M, Bayu G, Husain N, Rathore RK, Gupta RK (2007) Quantification of physiological and hemodynamic indices using T(1) dynamic contrast-enhanced MRI in intracranial mass lesions. *J Magn Reson Imaging* 26:871–80

St Lawrence KS, Lee TY (1998) An adiabatic approximation to the tissue homogeneity model for water exchange in the brain: I. Theoretical derivation.. *J Cereb Blood Flow Metab* 18:1365–77

Tofts PS (1997) Modeling tracer kinetics in dynamic Gd-DTPA MR imaging. *J Magn Reson Imaging* 7:91–101

Tofts PS, Brix G, Buckley DL, Evelhoch JL, Henderson E, Knopp MV, Larsson HB, Lee TY, Mayr NA, Parker GJ, Port RE, Taylor J, Weisskoff RM (1999) Estimating kinetic parameters from dynamic contrast-enhanced T(1)-weighted MRI of a diffusable tracer: standardized quantities and symbols. *J Magn Reson Imaging* 10: 223–32

Uematsu H, Maeda M, Sadato N, Matsuda T, Ishimori Y, Koshimoto Y, Kimura H, Yamada H, Kawamura Y, Yonekura Y, Itoh H (2001) Blood volume of gliomas determined by double-echo dynamic perfusion-weighted MR imaging: a preliminary study. *AJNR Am J Neuroradiol* 22:1915–9

Vonken EP, van Osch MJ, Bakker CJ, Viergever MA (2000) Simultaneous quantitative cerebral perfusion and Gd-DTPA extravasation measurement with dual-echo dynamic susceptibility contrast MRI. *Magn Reson Med* 43:820–7

Weisskoff RM, Boxerman JL, Sorensen AG, Kulke STC, Rosen BR (1994) Simultaneous blood volume and permeability mapping using a single Gd-based contrast injection. In: *Proceedings of the Second Annual Meeting of Society of Magnetic Resonance*. San Francisco, USA

Wu O, Ostergaard L, , Weisskoff RM, , Benner T, Rosen BR, Sorensen AG (2003) Tracer arrival timing-insensitive technique for estimating flow in MR perfusion-weighted imaging using singular value decomposition with a blockcirculant deconvolution matrix. *Magn Reson Med* 50:164–74